THE JOURNAL OF PHYSICAL CHEMISTRY C

Article

pubs.acs.org/JPCC

Optical Probe of Charge Separation at Organic/Inorganic Semiconductor Interfaces

H. Park,[†] M. Gutierrez,[‡] X. Wu,[†] W. Kim,[§] and X.-Y. Zhu*,[†]

[†]Department of Chemistry, Columbia University, New York, New York 10027, United States

[‡]Department of Chemistry & Biochemistry, University of Texas, Austin, Texas 78712, United States

[§]Korea Research Institute of Standards and Science, Yuseong, Daejeon 305-340, Korea

ABSTRACT: Organic/inorganic semiconductor heterojunctions are being explored in hybrid solar cells that take advantage of unique properties of both material systems. A key question concerns the mechanism of charge separation across the localized/delocalized semiconductor interface. Here we probe photoinduced charge transfer at a model interface between copper phthalocyanine (CuPc) and gallium arsenide (GaAs) by tracking the electric field on the femtosecond time scale using time-resolved second harmonic generation. For above bandgap excitation of GaAs, we resolve distinction channels of charge separation on 10^2 fs time scales: charge carrier separation in GaAs due to the delocalized space charge field and hole injection from photoexcited GaAs to localized CuPc molecular orbitals. At sufficiently high excitation density ($>10^{17}/cm^3$), charge separation by the space charge field leads to band flattening, which accelerates resonant hole transfer from GaAs to CuPc. We discuss implications of these findings to the design of organic/inorganic hybrid solar cells.

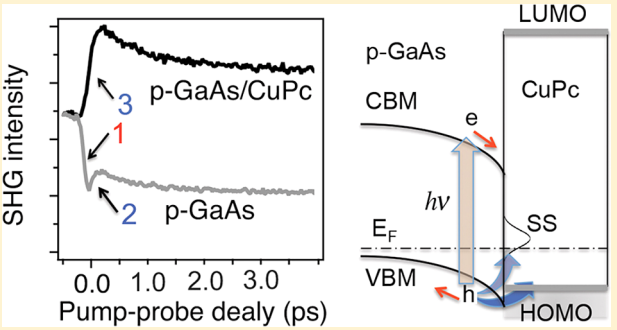

INTRODUCTION

Current photovoltaic technologies rely on inorganic semiconductors. The solar-to-electric power conversion efficiencies of single junction photovoltaics based on crystalline inorganic semiconductors can be as high as 28%, which is ~85% of the fundamental Shockley–Queisser limit.[1] However, these high-efficiency solar cells can be prohibitively expensive for large-scale implementations. In comparison, organic photovoltaics (OPVs), i.e., solar cells based on organic semiconductor materials (including conjugated polymers), can be produced and processed at low cost and on a very large scale. There is also growing interest in solar cells from hybrid organic/inorganic semiconductors that incorporate advantageous properties of both material systems, e.g., the high intrinsic carrier mobilities of inorganic semiconductors and the high optical density and broad optical tunability of organic semiconductors. In addition, molecule-specific photophysical processes, such as singlet exciton fission,[2] may be combined with inorganic semiconductors[3] to exceed the Shockley–Queisser limit. Hybrid solar cells based on organic materials and inorganic semiconductors in single crystal, thin film, or nanostructured formats have been demonstrated recently.[3−8] These solar cells rely on charge separation at the organic/inorganic semiconductor interface, but little is known about how such charge separation events occur. A fundamental question concerns how the distinctly different characteristics of charge carriers on the two sides of the interface determine the charge separation mechanisms. In most crystalline inorganic semiconductors, charge carriers move as free electrons or holes in the delocalized band structure, with charge separation determined by the space charge field at interfaces or p−n junctions. In organic semiconductors, optical excitation leads to localized excitons and charge separation requires energetic driving force resulting from energy level offset at electron donor/acceptor interfaces to form localized polarons in each phase.[9] At the hybrid organic/inorganic semiconductor interface, we do not know *a priori* if the delocalized, the localized, or both charge separation mechanisms operate and how these charge separation channels compete dynamically.

In order to answer the above questions, we choose the model system of copper phthalocyanine (CuPc) and gallium arsenide (GaAs). CuPc is the electron donor and hole transport material in the best-known small molecular organic photovoltaic cells (with fullerene as electron acceptor),[10] while GaAs is the inorganic semiconductor for single junction solar cells with the highest power conversion efficiency.[1] Hybrid CuPc/GaAs photovoltaic cells have been demonstrated before.[11] We probe photoinduced charge separation mechanism at the hybrid CuPc/GaAs interface using femtosecond time-resolved second harmonic generation (TR-SHG), particularly electric-field-induced SHG (EFISH).[12−16] EFISH is a four-wave mixing process in which two optical fields (ω) mix with a dc field (E_{dc}) to give signal at frequency 2ω. EFISH has been used to characterize static space charge fields at semiconductor

Received: March 25, 2013
Revised: May 7, 2013
Published: May 8, 2013

   dx.doi.org/10.1021/jp4029408 | J. Phys. Chem. C 2013, 117, 10974−10979

interfaces[14−16] and, in the time-resolved mode, to determine charge separation dynamics at semiconductor interfaces.[17−20] For the localized/delocalized semiconductor interface of CuPc/GaAs, we observe transient EFISH responses due to both charge carrier separation in GaAs by the space charge field and hole injection from photoexcited GaAs to localized CuPc molecular orbitals. These charge separation processes occur on the ultrafast time scales of ~10^2 fs and are cooperative at high excitation densities: band flattening resulting from charge separation in GaAs accelerates hole injection into CuPc by bring the holes in GaAs into resonance with CuPc molecular orbitals.

EXPERIMENTAL SECTION

We used highly doped ((1.0−1.2) × 10^{18}/cm^3) n-type (Si-doped) or p-type (Zn-doped) GaAs wafers with (001) surface termination (MTI Corporation). After cleaning in acetone and methanol, we etched each GaAs wafer in 30% aqueous NH_4OH for 5 min to remove the native oxide layer, followed by rinsing with deionized water. The etched surfaces were passivated with sulfur (S) in 20% aqueous $(NH_4)_2S$ for 2 h, followed by water rinse. The S-passivated GaAs samples were transferred into a vacuum chamber equipped with a thermal evaporator for the deposition of 10 nm CuPc, with film thickness calibrated by a quartz-crystal microbalance. The exact orientation of the CuPc molecules with respect to the GaAs surface is not known. Peisert et al. examined the orientation of CuPc thin films on a variety of solid surfaces and concluded that CuPc molecules adopt lying-down orientation only on clean single crystal metal or semiconductor surfaces, but in standing-up orientation on other technologically relevant surfaces, such as tin oxide, oxide-terminated silicon, and polycrystalline gold.[21] In view of this, we believe the CuPc thin film on the solution processed S-GaAs surface likely adopts the standing-up molecular orientation.

We characterized the energetic alignment at the interface by ultraviolet photoemission spectroscopy (UPS). UPS measurements were performed in an ultrahigh-vacuum chamber (UHV) with a base pressure of 10^{-9} Torr. UV light came from a helium discharge source (VG) with photon energies of 21.2 and 40.8 eV for He I and He II lines, respectively. Photoelectrons were detected on a hemispherical electron energy analyzer (VG 100AX).

A Ti:sapphire femtosecond oscillator (Coherent Mira 900) (800 nm wavelength, 76 MHz repetition rate, 110 fs pulse width) was used in the pump−probe SHG measurements. The laser pulse width allows us to obtain an experimental time resolution of approximately ±30 fs based on deconvolution. The incident pump and probe beams were p-polarized. The reflected probe beam was passed through a polarizer, a band-pass filter (400 nm), and a monochromator, and the second harmonic signal at 400 nm was detected by a photon counter. The angles of incidence of the pump and probe beams were 55° and 45°, respectively, from surface normal. In most measurements, the spot size and pulse energy on the surface were ~0.025 mm^2 and 3.6 nJ/pulse for the pump and ~0.01 mm^2 and 3.8 nJ/pulse for the probe. Zero delay was determined by autocorrelation measurements from the GaAs wafers. All optical experiments were performed in air at room temperature, and we found that the sample was stable over time due to the exceptional chemical and photochemical stability of CuPc. In TR-SHG measurements, the pump light at $h\nu$ = 1.55 eV selectively photoexcites GaAs (E_g = 1.4 eV), which is below the optical gap (= 1.76 eV) of CuPc.[19] Transient SHG signal is detected with a fundamental at $h\nu$ = 1.55 eV and the second harmonic at $h\nu$ = 3.10 eV.

RESULTS AND DISCUSSION

Static and Transient SHG from GaAs(001). GaAs is a noncentrosymmetric material and there is strong bulk SHG response.[14,22−24] Germer et al. characterized the SHG response from GaAs(001) using a phenomelogical model for the effective second-order nonlinear susceptibility, $\chi^{(2)}_{eff}$:

$$\chi^{(2)}_{eff} = \chi^{(2)} + 3\chi^{(3)}E_{dc} + 6\chi^{(4)}E_{dc}{}^2 + \ldots \quad (1)$$

where $\chi^{(2)}$, $\chi^{(3)}$, and $\chi^{(4)}$ are the second-, third-, and fourth-order nonlinear susceptibilities, respectively.[25] While the SHG response of GaAs is dominated by contributions from bulk $\chi^{(2)}$ and the first-order EFISH ($3\chi^{(3)}E_{dc}$) terms in eq 1, the bulk $\chi^{(2)}$ contribution can be minimized when one uses particular polarization combinations and sample orientation,[22] as shown by the static SHG signal from a native-oxide terminated GaAs(001) surface as a function of azimuthal angle (ϕ) from the (100) direction, with p-polarization for both incident fundamental and the second harmonic signal output (Figure 1A). Similar results are obtained for the S-passivated and CuPc-covered GaAs(001) surfaces. This azimuthal dependence shows a near 4-fold symmetry, as expected from the zinc-blende crystal structure of GaAs(001).[22] The small difference in the peak SHG intensity at ϕ = 45° or 225° from that at ϕ = 135° or 315° can be attributed to the interference between bulk, surface, and electric-field-induced (from the space charge region) SHG signals.[23,25] The SHG signal is minimized when the plane of incidence contains the (100) or (010) crystalline

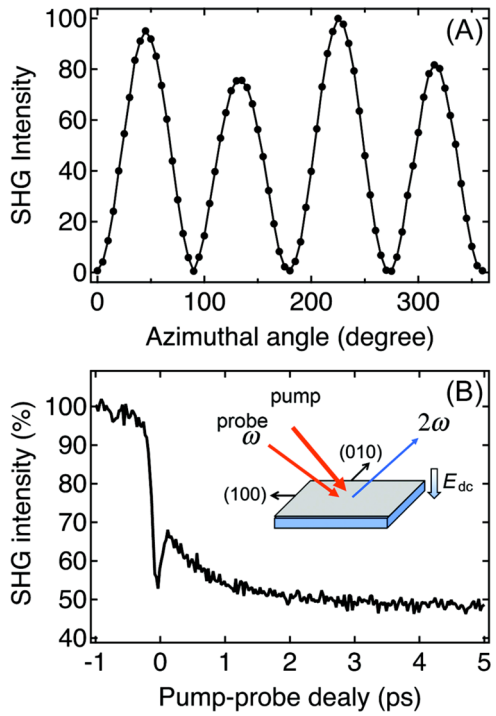

Figure 1. (A) Dependence of SHG intensity from a p-type GaAs wafer covered with a native oxide layer as a function of azimuthal angle (ϕ), which contains the plane of incidence and ϕ = 0 corresponds to the (100) crystal direction. (B) Normalized pump−probe SHG profile probed at ϕ = 0°. The inset illustrates schematically the pump−probe SHG experiment on the GaAs(001) surface.

dx.doi.org/10.1021/jp4029408 | J. Phys. Chem. C 2013, 117, 10974−10979

direction[23] and the magnitude of the signal at each minimum is nearly 3 orders of magnitude smaller than those at the maxima.

Further insight into the origins of SHG signal comes from pump−probe experiments in which the first laser pulse ($h\nu_1$ = 1.55 eV) excites electrons from the GaAs valence band to the conduction band and the second laser pulse probes the SHG response. Figure 1B shows time-resolved SHG profile probed at ϕ = 0°, i.e., the first minimum in Figure 1A. It is characterized by two features: (1) an ultrafast decrease in SHG intensity on the time scale of ∼100 ± 30 fs and (2) a subsequent rise of SHG intensity on the time scale of ∼200 ± 50 fs, followed by a slower decay characterized by an exponential time constant of ∼1.0 ± 0.2 ps. Here, feature 1 can be attributed to band flattening due to optical excitation. The near-surface region of GaAs features a space charge region due to band bending from charged surface states.[26,27] The initial optical excitation of photocarriers reduces the space charge field, i.e., band flattening due to the separation of photogenerated electron−hole pairs by the space charge field, followed by radiative recombination of photocarriers on much longer time scales, in excellent agreement with previous measurements on GaAs surfaces by electro-optic sampling,[28] transient reflectance,[29] and SHG.[30] Note that the coherent phonons observed in previous measurements[29,30] are not resolved in Figure 1 due to the longer laser pulses used here. The time scale (∼200 fs) of the second feature is consistent with the ultrafast dynamics of trapping of photocarriers by surface states.[31,32] In this case, it is the trapping of photoholes by filled surface states; this process increases the electric field in the same direction as the space charge field for p-GaAs and, thus, increases the EFISH contribution to the SHG intensity. The subsequent decay of SHG signal can then be attributed to surface state mediated recombination of photocarriers. The above interpretation suggests the dominant role of EFISH contribution to pump-induced SHG signal; this interpretation is verified by pump-induced SHG responses at the GaAs/CuPc interfaces, as detailed below. Note that the relative magnitudes of the two features in time-resolved SHG responses depend on light polarization and azimuthal angle. A detailed analysis of the various tensor elements for the SHG responses at the GaAs(001) surface is beyond the scope of this report and will be published later. In the following, we focus on charge separation dynamics at CuPc/GaAs(001) interfaces probed at ϕ = 0°.

Electronic Energy Level Alignment at CuPc/GaAs(001) Interfaces. We establish electronic energy level alignment at the CuPc/GaAs interface using UPS, which reveals the pinning of the surface Fermi level in the middle of the bandgap on both p- and n-type GaAs(001) surfaces with sulfur passivation, in agreement with previous reports.[33,34] This gives rise to opposite band bending directions for the p- and n-type GaAs, respectively. We can estimate the magnitudes of band bending for the p- and n-type GaAs surfaces. When the doping concentration is ∼10^{18} cm^{-3} in GaAs, the Fermi levels are approximately given by $E_F - E_V = kT[\log(N_V/n_p)]$ and $E_F - E_c = kT[\log(n_n/N_c) + 0.354(n_n/N_c)]$ for the nondegenerate p-GaAs and the degenerate n-GaAs, respectively.[35] Here, n_p and n_n are the doping concentrations in p- and n-type GaAs, respectively; N_V and N_C are the effective density of states in the valence and conduction bands of GaAs, respectively. The calculated Fermi levels are 0.057 eV above the VBM in p-GaAs and 0.039 eV above the CBM in n-GaAs. Therefore, the magnitude of the band bending is about 0.54 eV for p-GaAs and 0.74 eV for n-GaAs, in agreement with UPS measurements detailed below.

Because of the presence of bandgap surface states, it is difficult to accurately determine the valence band maximum (VBM) of the GaAs surface from the GaAs valence band in UPS. Following the work of Yu et al.,[33] we reference the VBM to the Ga_{3d} core level, as shown in Figure 2C for the p-GaAs:S surface without or with CuPc overlayers. The binding energies (referenced to the Fermi level) of Ga_{3d} are found at 19.3 ± 0.1 and 19.4 ± 0.1 eV for p- and n-type GaAs, respectively. These results put the CBM at 0.4 ± 0.1 and 0.5 ± 0.1 eV for p- and n-type GaAs(001):S, respectively, in agreement with the estimated band bending.

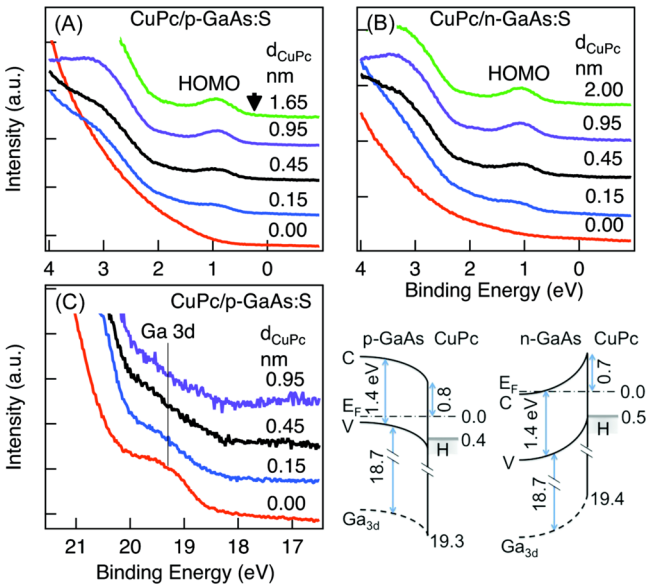

Figure 2. He I ultraviolet photoemission spectra (UPS) from (A) p-GaAs:S and (B) n-GaAs:S with CuPc overlay of film thicknesses (bottom to top, d_{CuPc} = 0.00 to 1.65 or 2.00 nm). The arrow in (A) marks the threshold position for CuPc HOMO. (C) He II UPS from p-GaAs:S with CuPc overlay film thickness (bottom to top) of d_{CuPc} = 0.00−0.95 nm. The lower right shows schematically the electronic energy level alignment at the CuPc/GaAs interfaces. C: CBM; V: VBM; H: HOMO; E_F: Fermi level.

With the deposition of a CuPc thin film on the S-passivated GaAs(001) surface, the highest occupied molecular orbital (HOMO) of CuPc appears near the VBM of GaAs, as shown in Figure 2A,B for increasing CuPc thickness on p- and n-GaAs:S, respectively. Following common practice, we use the upper threshold (arrow in Figure 2A) of the HOMO peak to indicate the HOMO position, which is at ∼0.2 eV above the surface VBM of GaAs, regardless of dopant type. Note that the band alignments probed here for CuPc on S-passivated GaAs(001) differ from those reported for CuPc on the clean GaAs(001) surfaces,[36] as expected for III−V semiconductors with different surface conditions.[34] The lower-right panel in Figure 2 summarizes the energy level diagrams for the GaAs/CuPc interfaces.

Charge Separation Dynamics at CuPc/GaAs(001) Interfaces. We compare pump−probe SHG profiles obtained from S-passivated n-GaAs(001) (orange curve in Figure 3B) with that from p-GaAs(001) (orange curve in Figure 3A). Similar to that for p-GaAs, we see an initial decrease in SHG intensity following photoexcitation of n-GaAs due to band

dx.doi.org/10.1021/jp4029408 | J. Phys. Chem. C 2013, 117, 10974−10979

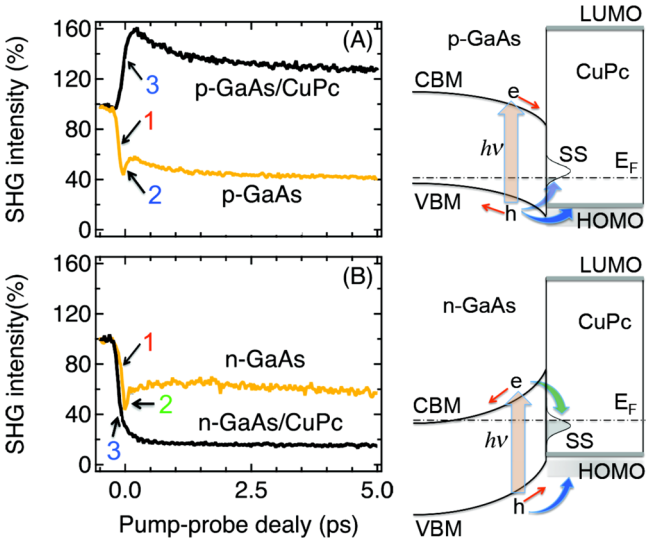

Figure 3. Right: schematic energy level diagrams at p- (upper) an n-type (lower) GaAs/CuPc interfaces, as determined from ultraviolet photoemission spectroscopy (UPS). The magnitude of band bending in the near surface region of S-passivated GaAs is not changed upon CuPc deposition. The arrows represent optical excitation (red), hole (light blue), or electron (green) trapping by surface states and hole injection into CuPc (blue). Left: pump−probe SHG profiles measured at ϕ = 0° for S-passivated GaAs surfaces (orange curves) and the S-GaAs surfaces with a 10 nm CuPc thin film deposited on top. Panels A and B are for p- and n-type GaAs, respectively. The SHG intensity is normalized to that before the arrival of the pump pulse in each case. The features indicated by the arrows with colored numbers correspond to the colored arrows in the schematics on the right: (1) band flattening, (2) photocarrier trapping by surface states, and (3) hole injection from GaAs to CuPc.

flattening. This is again followed by an ultrafast rise in SHG signal attributable to the trapping of photoexcited conduction band electrons by surface states and subsequent slower decay due to surface-state-mediated recombination, as detailed below. On GaAs surfaces, the different directions of band bending explains why ultrafast trapping of photocarriers by surface states occurs for valence band holes on p-type GaAs and conduction band electrons on n-type GaAs. In each case, the carrier being trapped is energetically resonant with the surface state while the opposite carrier is not. At CuPc/GaAs(001) interfaces, the energy level diagrams in Figure 2 also predict that above band gap photoexcitation of GaAs (n- or p-type) should permit hole injection, but not electron injection, into CuPc. This is verified in TR-SHG measurements.

The black curves in the left panels of Figure 3 are pump−probe SHG profiles for S-passivated p- (A) and n-type (B) S-passivated GaAs(001) surfaces with a 10 nm CuPc thin film deposited on top. We first focus on p-type GaAs/CuPc. Instead of the decrease in SHG intensity upon optical excitation of the bare p-GaAs surface, the p-GaAs/CuPc interface shows an ultrafast increase in SHG intensity upon optical excitation of GaAs. Given the electronic energy level alignment determined in Figure 2, we assign this increase in interfacial electric field to hole injection from photoexcited GaAs to CuPc. This hole injection leads to an interfacial electric field in the same direction as the space charge field on p-GaAs, leading to pump-induced increase in interfacial electric field. Since band flattening of the inorganic semiconductor is still present upon above-bandgap excitation of GaAs, the magnitude of the electric field increase due to hole injection into CuPc at the hybrid GaAs/CuPc interface must be dominant under the experimental conditions used here. This interpretation leads us to predict that, for the n-GaAs/CuPc interface, hole injection from photoexcited GaAs to CuPc should lead to interfacial electric field in the opposite direction as the space charge field. Thus, both band flattening in GaAs and hole transfer from n-GaAs to CuPc should result in decreases in SHG intensity. This prediction is verified by the pump−probe SHG profile for the n-GaAs/CuPc interface (black curve in Figure 3B). Photoexcitation of n-GaAs at the n-GaAs/CuPc interface results in an ultrafast decrease in SHG intensity, with the magnitude of the decrease larger than that on bare n-GaAs. Note that the small increase in SHG intensity attributed to electron trapping by surface state is not observed at the n-GaAs/CuPc interface. The minor channel of surface state trapping is likely quenched at the GaAs/CuPc interface. The various dynamic processes of charge separation are summarized schematically on the right side of Figure 3.

The findings presented above reveal two major charge separation channels at GaAs/CuPc interfaces: (1) separation of photo carriers in GaAs by the space charge field and (2) transfer of photogenerated hole from the valence band of GaAs to CuPc. The latter gives opposite results on interfacial fields for the two doping types. On n-GaAs, the hole injection channel decreases the space charge field in the same direction as the band-flattening effect. On p-GaAs, hole injection creates an interfacial electric field in the same direction as the original space charge field and, thus, has an opposite effect on SHG intensity as band flattening does.

Since the band flattening effect saturates at a photocarrier density on the order of the trap density (10^{11-13}/cm^2) on the GaAs(001) surface,[26,27] while hole injection density from GaAs to CuPc could be much higher, we predict that the relative contributions of the two charge separation channels should depend on excitation density (and thus laser power). This prediction is indeed verified. Figure 4A shows pump−probe SHG responses for the p-GaAs/CuPc interface at different

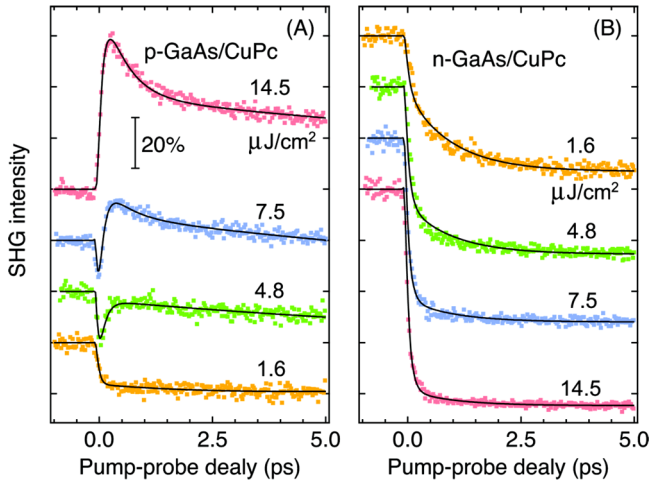

Figure 4. Pump−probe SHG profiles measured at ϕ = 0° for (A) p-GaAs/CuPc and (B) n-GaAs/CuPc interfaces measured with different pump pules energy densities (1.6−14.5 μJ/cm^2). Color dots are experimental data, and black curves are kinetic fits. The SHG intensity is normalized to that before the arrival of the pump pulse in each case, and percentage change is indicated in panel A. The profiles are offset vertically for clarity.

dx.doi.org/10.1021/jp4029408 | J. Phys. Chem. C 2013, 117, 10974−10979

pump laser pules energy densities (I). At the lowest pules energy density of I = 1.6 μJ/cm^2, corresponding to a bulk excitation density of $\rho_e \sim 10^{17}$ cm^{-3} as estimated from the extinction coefficient of GaAs, we see only pump-induced decrease in SHG intensity, suggesting the band-flattening effect dominates, and there is no evidence for hole injection. As the pump power increases, we clearly see the appearance of the hole injection channel (the rise in SHG intensity). At the highest pules energy density of I = 14.5 μJ/cm^2, (bulk excitation density $\rho_e \sim 10^{18}$ cm^{-3}), there is only increase in pump-induced SHG intensity and, thus, hole injection overwhelms band flattening. The fact that hole injection to CuPc is more evident for bulk excitation density $\rho_e > 10^{17}$ cm^{-3} suggests that band flattening assists hole transfer. This is easily understood from the schematic in Figure 3. For p-type GaAs, charge separation by the space charge field moves the photoexcited holes into the bulk of GaAs; as a result, hole injection into CuPc on the GaAs surface is inhibited. When the excitation density is sufficiently high (>10^{17} cm^{-3}), the initial band bending is lifted (i.e., band flattening) and hole injection across the interface becomes important. In comparison, both band flattening and hole injection decrease electric field on n-GaAs. As a result, we see only pump-induced decrease in SHG intensity at the n-GaAs/CuPc interface, independent of excitation density in the excitation density used (Figure 4B).

While a quantitative analysis of TR-SHG profiles is difficult due to nonlinear responses of the two dominant contributions to interfacial electric field as functions of excitation density, we can qualitatively estimate the time scales of these processes. We treat the total pump-induced SHG response from each GaAs/CuPc interface as a sum of two EFISH contributions: (1) charge separation in GaAs by the space charge field and (2) charge separation at the interface due to hole injection from GaAs to CuPc. The first contribution, which dominates the initial decrease in SHG intensity following the photoexcitation of S-passivated p-GaAs (orange curve in Figure 3A) or p-GaAs/CuPc interface at low excitation density (~10^{17} cm^{-3}, orange curve in Figure 4A), is characterized by a single-exponential charge separation time constant of $\tau_{CS} \sim 90 \pm 30$ fs. For the p-GaAs/CuPc interface at an excitation density >10^{17} cm^{-3}, we add a single-exponential lifetime of τ_{hi} for ultrafast hole injection and single (or bi-) exponential lifetime for charge recombination on longer time scales. We convolute this two-component kinetic model with the laser excitation cross-correlation profile approximated by a Gaussian function with full width at half-maximum (fwhm) of 156 fs (corresponding to a laser pulse width of 110 fs). The solid curves in Figure 4 show fits to this simple kinetic model. At the p-GaAs/CuPc interface, the fits yield a hole injection time of $\tau_{hi} \sim 120 \pm 30$ fs, independent of excitation density for $\rho_e > 10^{17}$ cm^{-3}. For the S-passivated n-GaAs surface (orange curve in Figure 3B) or n-GaAs/CuPc interfaces (Figure 4B), the time constant for the initial band flattening is also $\tau_{CS} \sim 90 \pm 30$ fs. At the n-GaAs/CuPc interface, in addition to the fast channel of charge separation by the space charge field, we observe at low excitation densities a slow dynamic channel (orange curve in Figure 4B), which is characterized by a single-exponential time constant of $\tau_{hi} \sim 1.1 \pm 0.2$ ps. With increasing pump density, the hole-injection channel is accelerated to the point of being indistinguishable from τ_{CS}. Given the energy level diagram for n-GaAs/CuPc in Figure 2, we attribute the acceleration of interfacial hole injection with increasing excitation density to the band-flattening effect, which brings most photoexcited holes in the GaAs valence band into resonance with the HOMO of CuPc.

CONCLUSIONS

The finding presented above reveals the presence of competing charge separation processes at the model GaAs/CuPc inorganic/organic semiconductor interface. For above bandgap excitation of GaAs, we resolve distinct channels of charge carrier separation driven by (i) the delocalized space charge field in GaAs and (ii) charge transfer from GaAs to localized CuPc due to an energetic driving force at the interface. The dynamic competition between these two distinct charge separation pathways depends on not only doping type (and thus band-bending direction) in the delocalized inorganic semiconductors but also energetic alignment at the inorganic/organic semiconductor interface. On both p- and n-GaAs, the presence of the space charge field slows down hole injection from GaAs to CuPc. At higher excitation density (>10^{17} cm^{-3}), band flattening brings the GaAs valence band to closer resonance with the CuPc HOMO, and hole injection to CuPc is accelerated. However, this excitation density is ~10^{3-4} higher than that achievable with solar radiation (~1 kW/m^2). Thus, the band-flattening effect cannot be realized without unrealistic solar concentration. When designing hybrid solar cells based on organic/inorganic semiconductor interfaces, controlling surface state density and thus the magnitude of band-bending on the inorganic semiconductor surface is of critical importance to the optimization of charge separation efficiency.

AUTHOR INFORMATION

Corresponding Author

*E-mail: xyzhu@columbia.edu (X.-Y.Z.).

Notes

The authors declare no competing financial interest.

ACKNOWLEDGMENTS

This work was supported by the National Science Foundation SOLAR Collaborative: Designing and modeling advanced nanostructure based hybrid solar cells, grant DMR-1125845. J.W.K. was supported by MEST and PAL, the XFEL project, Korea. We thank Dr. Ramesh Laghumavarapu of UCLA for help with GaAs sample preparation.

REFERENCES

(1) Green, M. A.; Emery, K.; Hishikawa, Y.; Warta, W.; Dunlop, E. D. Solar Cell Efficiency Tables (Version 39). *Prog. Photovolt: Res. Appl.* **2012**, *20*, 12−20.

(2) Chan, W.-L.; Ligges, M.; Jailaubekov, A.; Kaake, L.; Miaja-Avila, L.; Zhu, X.-Y. Observing the Multiexciton State in Singlet Fission and Ensuing Ultrafast Multielectron Transfer. *Science* **2011**, *334*, 1541−1545.

(3) Ehrler, B.; Walker, B. J.; Böhm, M. L.; Wilson, M. W. B.; Vaynzof, Y.; Friend, R. H.; Greenham, N. C. In Situ Measurement of Exciton Energy in Hybrid Singlet-fission Solar Cells. *Nat. Commun.* **2012**, *3*, 1019/1−6.

(4) Greenham, N.; Peng, X.; Alivisatos, A. P. Charge Separation and Transport in Conjugated-Polymer/Semiconductor-Nanocrystal Composites Studied by Photoluminescence Quenching and Photoconductivity. *Phys. Rev. B* **1996**, *54*, 17628−17637.

(5) Huynh, W. U.; Dittmer, J. J.; Alivisatos, A. P. Hybrid Nanorod-Polymer Solar Cells. *Science* **2002**, *295*, 2425−2447.

(6) Lancelle-Beltran, E.; Prené, P.; Boscher, C.; Belleville, P.; Buvat, P.; Sanchez, C. All-Solid-State Dye-Sensitized Nanoporous TiO_2

Hybrid Solar Cells with High Energy-Conversion Efficiency. *Adv. Mater.* **2006**, *18*, 2579−2582.
(7) Oosterhout, S. D.; Wienk, M. M.; van Bavel, S. S.; Thiedmann, R.; Jan Anton Koster, L.; Gilot, J.; Loos, J.; Schmidt, V.; Janssen, R. A. J. The Effect of Three-Dimensional Morphology on the Efficiency of Hybrid Polymer Solar Cells. *Nat. Mater.* **2009**, *8*, 818−824.
(8) Herrmann, D.; Niesar, S.; Scharsich, C.; Köhler, A.; Stutzmann, M.; Riedle, E. Role of Structural Order and Excess Energy on Ultrafast Free Charge Generation in Hybrid Polythiophene/Si Photovoltaics Probed in Real Time by Near-Infrared Broadband Transient Absorption. *J. Am. Chem. Soc.* **2011**, *133*, 18220−18233.
(9) Clarke, T. M.; Durrant, J. R. Charge Photogeneration in Organic Solar Cells. *Chem. Rev.* **2010**, *110*, 6736−6767.
(10) Xue, J.; Rand, B. P.; Uchida, S.; Forrest, S. R. A Hybrid Planar-Mixed Molecular Heterojunction Photovoltaic Cell. *Adv. Mater.* **2005**, *17*, 66−71.
(11) Karimov, Kh. S.; Ahmed, M. M.; Moiz, S. A.; Fedorov, M. I. Temperature-Dependent Properties of Organic-on-Inorganic Ag/p-CuPc/n-GaAs/Ag Photoelectric Cell. *Sol. Energy Mater. Sol. Cells* **2005**, *87*, 61−75.
(12) Lee, C. H.; Chang, R. K.; Bloembergen, N. Nonlinear Electroreflectance in Silicon and Silver. *Phys. Rev. Lett.* **1967**, *18*, 167−170.
(13) Zhao, X. L.; Ong, S. W.; Wang, H. F.; Eisenthal, K. B. New Method for Determination of Surface pKa Using Second Harmonic Generation. *Chem. Phys. Lett.* **1993**, *214*, 203−207.
(14) Qi, J.; Yeganeh, M. S.; Koltover, I.; Yodh, A. G.; Theis, W. M. Depletion-Electric-Field-Induced Changes in Second-Harmonic Generation from GaAs. *Phys. Rev. Lett.* **1993**, *71*, 633−636.
(15) Aktsipetrov, O. A.; Fedyanin, A. A.; Golovkina, V. N.; Murzina, T. V. Optical Second-Harmonic Generation Induced by a DC Electric Field at the Si-SiO_2 Interface. *Opt. Lett.* **1994**, *19*, 1450−1452.
(16) Bloch, J.; Mihaychuk, J.; van Driel, H. Electron Photoinjection from Silicon to Ultrathin SiO_2 Films via Ambient Oxygen. *Phys. Rev. Lett.* **1996**, *77*, 920−923.
(17) Glinka, Y. D.; Shahbazyan, T. V.; Perakis, I. E.; Tolk, N. H.; Liu, X.; Sasaki, Y.; Furdyna, J. K. Ultrafast Dynamics of Interfacial Electric Fields in Semiconductor Heterostructures Monitored by Pump-Probe Second-Harmonic Generation. *Appl. Phys. Lett.* **2002**, *81*, 3717−3719.
(18) Tisdale, W. A.; Williams, K. J.; Timp, B. A.; Norris, D. J.; Aydil, E. S.; Zhu, X.-Y. Hot-Electron Transfer from Semiconductor Nanocrystals. *Science* **2010**, *328*, 1543−1547.
(19) Kaake, L.; Jailaubekov, A.; Williams, K. J.; Zhu, X.-Y. Probing Ultrafast Charge Separation at Organic Donor/Acceptor Interfaces by a Femtosecond Electric Field Meter. *Appl. Phys. Lett.* **2011**, *99*, 083307.
(20) Jailaubekov, A.; Willard, A. P.; Tritsch, J.; Chan, W.-L.; Sai, N.; Kaake, L.; Gearba, R. I.; Leung, K.; Rossky, P. J.; Zhu, X.-Y. Hot Charge-Transfer Excitons Set the Time Limit for Charge Separation at Donor/Acceptor Interfaces in Organic Photovoltaics. *Nat. Mater.* **2013**, *12*, 66−73.
(21) Peisert, H.; Schwieger, T.; Auerhammer, J. M.; Knupfer, M.; Golden, M. S.; Fink, J.; Bressler, P. R.; Mast, M. Order on Disorder: Copper Phthalocyanine Thin Films on Technical Substrates. *J. Appl. Phys.* **2001**, *90*, 466−469.
(22) Stehlin, T.; Feller, M.; Guyot-Sionnest, P.; Shen, Y. R. Optical Second-Harmonic Generation as a Surface Probe for Noncentrosymmetric Media. *Opt. Lett.* **1988**, *13*, 389−391.
(23) Yamada, C.; Kimura, T. Anisotropy in Second-Harmonic Generation from Reconstructed Surfaces of GaAs. *Phys. Rev. Lett.* **1993**, *70*, 2344−2347.
(24) Bergfeld, S.; Daum, W. Second-Harmonic Generation in GaAs: Experiment versus Theoretical Predictions of $\chi_{xyz}^{(2)}$. *Phys. Rev. Lett.* **2003**, *90*, 036801.
(25) Germer, T. A.; Kołasin-acuteski, K. W.; Stephenson, J. C.; Richter, L. J. Depletion-Electric-Field-Induced Second-Harmonic Generation Near Oxidized GaAs(001) Surfaces. *Phys. Rev. B* **1997**, *55*, 10694.
(26) Yin, X.; Chen, H.-M.; Pollak, F. H.; Chan, Y.; Montano, P. A.; Kirchner, P. D.; Pettit, G. D.; Woodall, J. M. Photoreflectance Study of the Surface Fermi Level at (001) N- and P-type GaAs Surfaces. *J. Vac. Sci. Technol. A* **1992**, *10*, 131−136.
(27) Chang, G. S.; Hwang, W. C.; Wang, Y. C.; Yang, Z. P.; Hwang, J. S. Determination of Surface State Density for GaAs and InAlAs by Room Temperature Photoreflectance. *J. Appl. Phys.* **1999**, *86*, 1765−1767.
(28) Min, L.; Miller, R. J. D. Picosecond Electro-Optic Sampling of Electron-Hole Vertical Transport in Surface Space Charge Fields. *Chem. Phys. Lett.* **1989**, *163*, 55−60.
(29) Cho, G.; Kütt, W.; Kurz, H. Subpicosecond Time-Resolved Coherent-Phonon Oscillations in GaAs. *Phys. Rev. Lett.* **1990**, *65*, 764−766.
(30) Chang, Y.; Xu, L.; Tom, H. Observation of Coherent Surface Optical Phonon Oscillations by Time-Resolved Surface Second-Harmonic Generation. *Phys. Rev. Lett.* **1997**, *78*, 4649−4652.
(31) Lanzafame, J. M.; Palese, S.; Wang, D.; Miller, R. J. D.; Muenter, A. A. Ultrafast Nonlinear Optical Studies of Surface Reaction Dynamics: Mapping the Electron Trajectory. *J. Phys. Chem.* **1994**, *98*, 11020−11033.
(32) Kang, J. U.; Frankel, M. Y.; Huang, J.-W.; Kuech, T. F. Ultrafast Carrier Trapping in Oxygen-Doped Metal-Organic Vapor Phase Epitaxy GaAs. *Appl. Phys. Lett.* **1997**, *70*, 1560−1562.
(33) Yu, E. T.; Chow, D. H.; McGill, T. C. Commutativity of the GaAs/AlAs (100) Band Offset. *J. Vac. Sci. Technol. B* **1989**, *7*, 391−394.
(34) Helander, M. G.; Greiner, M. T.; Wang, Z. B.; Lu, Z. H. Band Alignment at the Hybrid Heterojunction Between S-Passivated III−V Semiconductors and C_{60}. *J. Appl. Phys.* **2009**, *106*, 056105.
(35) Sze, S. M.; Ng, K. K. *Physics of Semiconductor Devices*; Wiley-Interscience: New York, 2006.
(36) Ding, H.; Gao, Y.; Cinchetti, M.; Wüstenberg, J.-P.; Sánchez-Albaneda, M.; Andreyev, O.; Bauer, M.; Aeschlimann, M. Spin Injection and Spin Dynamics at the CuPc/GaAs Interface Studied With Ultraviolet Photoemission Spectroscopy and Two-Photon Photoemission Spectroscopy. *Phys. Rev. B* **2008**, *78*, 075311.